Rosa Escutia, Á.; Gutierrez Campo, AM.; Brimont, ACJ.; Griol Barres, A.; Sanchis Kilders, P. (2016). High performace silicon 2x2 optical switch based on a thermo-optically tunable multimode interference coupler and efficient electrodes. Optics Express. 24(1):191-198. doi:10.1364/OE.24.000191.

High performace silicon 2x2 optical switch based on a thermo-optically tunable multimode interference coupler and efficient electrodes

Álvaro Rosa, Ana Gutiérrez, Antoine Brimont, Amadeu Griol, and Pablo Sanchis

*

Abstract: Optical switches based on tunable multimode interference (MMI) couplers can simultaneously reduce the footprint and increase the tolerance against fabrication deviations. Here, a compact 2x2 silicon switch based on a thermo-optically tunable MMI structure with a footprint of only 0.005mm^2 is proposed and demonstrated. The MMI structure has been optimized using a silica trench acting as a thermal isolator without introducing any substantial loss penalty or crosstalk degradation. Furthermore, the electrodes performance have significantly been improved via engineering the heater geometry and using two metallization steps. Thereby, a drastic power consumption reduction of around 90% has been demonstrated yielding to values as low as 24.9 mW. Furthermore, very fast switching times of only 1.19 μs have also been achieved.

References and links

1. H. Subbaraman, X. Xu, A. Hosseini, X. Zhang, Y. Zhang, D. Kwong, and R. T. Chen, "Recent advances in silicon-based passive and active optical interconnects," Opt. Express **23**(3), 2487–2510 (2015).
2. D. Nikolova, S. Rumley, D. Calhoun, Q. Li, R. Hendry, P. Samadi, and K. Bergman, "Scaling silicon photonic switch fabrics for data center interconnection networks," Opt. Express **23**(2), 1159–1175 (2015).
3. P. Dong, S. F. Preble, and M. Lipson, "All-optical compact silicon comb switch," Opt. Express **15**(15), 9600–9605 (2007).
4. A. Biberman, H. L. R. Lira, K. Padmaraju, N. Ophir, J. Chan, S. Member, M. Lipson, S. Member, and K. Bergman, "Broadband silicon photonic electrooptic switch for photonic interconnection networks," IEEE Photonics Technol. Lett. **23**(8), 504–506 (2011).
5. G. Li, X. Zheng, J. Yao, H. Thacker, I. Shubin, Y. Luo, K. Raj, J. E. Cunningham, and A. V. Krishnamoorthy, "25Gb/s 1V-driving CMOS ring modulator with integrated thermal tuning," Opt. Express **19**(21), 20435–20443 (2011).
6. A. Densmore, S. Janz, R. Ma, J. H. Schmid, D.-X. Xu, A. Delâge, J. Lapointe, M. Vachon, and P. Cheben, "Compact and low power thermo-optic switch using folded silicon waveguides," Opt. Express **17**(13), 10457–10465 (2009).
7. J. Van Campenhout, W. M. J. Green, S. Assefa, and Y. A. Vlasov, "Low-power, 2 × 2 silicon electro-optic switch with 110-nm bandwidth for broadband reconfigurable optical networks," Opt. Express **17**(26), 24020–24029 (2009).
8. P. Dong, S. Liao, H. Liang, R. Shafiiha, D. Feng, G. Li, X. Zheng, A. V. Krishnamoorthy, and M. Asghari, "Submilliwatt, ultrafast and broadband electro-optic silicon switches," Opt. Express **18**(24), 25225–25231 (2010).
9. P. Sun and R. M. Reano, "Submilliwatt thermo-optic switches using free-standing silicon-on-insulator strip waveguides," Opt. Express **18**(8), 8406–8411 (2010).
10. M. R. Watts, J. Sun, C. DeRose, D. C. Trotter, R. W. Young, and G. N. Nielson, "Adiabatic thermo-optic Mach-Zehnder switch," Opt. Lett. **38**(5), 733–735 (2013).
11. N. C. Harris, Y. Ma, J. Mower, T. Baehr-Jones, D. Englund, M. Hochberg, and C. Galland, "Efficient, compact and low loss thermo-optic phase shifter in silicon," Opt. Express **22**(9), 10487–10493 (2014).
12. K. Suzuki, G. Cong, K. Tanizawa, S.-H. Kim, K. Ikeda, S. Namiki, and H. Kawashima, "Ultra-high-extinction-ratio 2 × 2 silicon optical switch with variable splitter," Opt. Express **23**(7), 9086–9092 (2015).
13. L. Sanchez, A. Griol, S. Lechago, A. Brimont, and P. Sanchis, "Low-power operation in a silicon switch based on an asymmetric Mach-Zehnder interferometer," IEEE Photonics J. **7**(2), 1–8 (2015).

14. P. A. Besse, M. Bachmann, H. Melchior, L. B. Soldano, and M. K. Smit, "Optical bandwidth and fabrication tolerances of multimode interference couplers," J. Lightwave Technol. **12**(6), 1004–1009 (1994).
15. L. Soldano and E. Pennings, "Optical multi-mode interference devices based on self-imaging: principles and applications," J. Lightwave Technol. **13**(4), 615–627 (1995).
16. J. Leuthold and C. H. Joyner, "Multimode interference couplers with tunable power splitting ratios," J. Lightwave Technol. **19**(5), 700–707 (2001).
17. D. A. May-Arrioja and P. Likamwa, "Reconfigurable 3-dB MMI splitter," in *Proc. IEEE/LEOS Summer Topical Meetings* (IEEE, 2008), pp. 21–23.
18. F. Wan, J. Yang, L. Chen, X. Jiang, and M. Wang, "Optical switch based on multimode interference coupler," IEEE Photonics Technol. Lett. **18**(2), 421–423 (2006).
19. Á. Rosa, A. Brimont, A. Griol, and P. Sanchis, "Optimized micro-heater structures for tunable silicon multimode interferometers," in *Proc. IEEE Group IV Photonics* (IEEE, 2014), pp. 91–92.
20. Á. Rosa, A. Griol, A. M. Gutierrez, A. Brimont, and P. Sanchis, "Silicon 2x2 optical switch based on optimized multimode interference coupler to minimize power consumption," in *European Conference on Optical Communications* (2015), paper P.2.17.
21. A. Wasserman, *Thermal Physics: Concepts and Practice* (Cambridge University, 2012).

1. Introduction

Next-generation optical networks will need to deal with low power consumption, low latency and high bandwidth requirements in order to exceed the current performance of electrical networks. As a result, silicon photonics is probably the most promising technology to provide these characteristics for short range communications, on chip scale communications and in the future to intra-chip communications [1]. Optical switches are one of the core building blocks in optical networks. Until now, silicon switches have been mostly based on two different photonic structures: ring resonators and Mach-Zehnder interferometric (MZI) structures. Ring resonators allow minimizing the footprint but at expenses of a narrow optical bandwidth which can only be increased by using more complex ring structures or switching techniques [2–4]. Furthermore, an additional tuning mechanism, which will increase the total power consumption, is also necessary to counteract possible fabrication deviations [5]. On the other hand, silicon MZI switches have a wider optical bandwidth and higher robustness but usually suffer from a larger footprint and higher power consumption that limits the scalability to build switching fabrics with a large number of ports [6–13].

Optical switches based on multimode interferometers (MMIs) could provide both small footprint and relaxed fabrication tolerances [14–16]. Tunability in MMIs have been reported for different material technologies like InGaAsP [17] and polymers [18]. However, tunability in silicon MMIs has only been recently demonstrated by means of the thermo-optic effect [19, 20]. The reduction of power consumption has been investigated by engineering the electrical and optical parts of the switching device. In the former, the optimization of the heater geometry has been proposed to improve the efficiency of the thermal process but power consumption was only reduced to 65 mW [19]. On the other hand, a power consumption reduction of around 50% has also been demonstrated by designing a thermal isolating silica trench within the MMI optical structure but a high power consumption of 120mW was still measured [20]. In this work, we report a high performance 2x2 MMI silicon switch by combining both concepts and by using two metallization steps for the electrodes. Thereby, a drastic power consumption reduction of around 90% has been demonstrated yielding to values as low as 24.9 mW. Furthermore, very fast switching times of only 1.19 μs have also been achieved.

2. Design of the MMI switch

The proposed MMI switch is composed by a multimode silicon waveguide connected to two tapered output and input ports. The tapered ports minimize return losses and provide a wider excitation input and therefore larger self-images into the MMI section. Larger self-images reduce the index variation for switching the MMI, which gives rise to a reduction in power consumption.

The MMI parameters have been designed taking into account the tapered ports. A length, L_{MMI}, of 594.5 µm and a width, W_{MMI}, of 9 µm have been obtained thus giving rise to a compact footprint of around 0.005 mm^2. Switching is achieved by inducing a π-phase shift of one of the two self-images located under the electrodes at $L_{MMI}/2$ (see sketch in Fig. 1(a)). This phase shift results in a new mirrored interference pattern that propagates after the electrode [16].

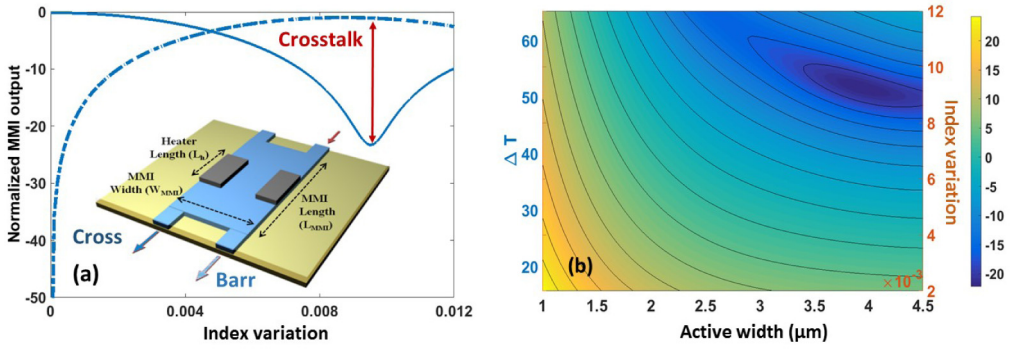

Fig. 1. (a) Sketch of the tunable MMI and transmission response as a function of the index variation. (b) Crosstalk dependence on the width of the active area where the silicon index is changed.

The relationship between phase and index change may be estimated as:

$$\Delta\phi = k \cdot \Delta n \cdot L_h \tag{1}$$

where L_h is the heater length to achieve the required phase shift and $k = 2\pi/\lambda$ is the wavelength number. The index change, Δn, is determined by the thermal coefficient, $\partial n/\partial T$, of the material, in this case, silicon, and can be calculated as:

$$\Delta n = \frac{\partial n}{\partial T} \cdot \Delta T \tag{2}$$

where the thermal coefficient for silicon is $1.84 \cdot 10^{-4}$ K^{-1}. Thereby, a compact heater of 80 µm length can be used to achieve a π-phase shift if the index change is around $\Delta n \approx 10^{-2}$, which would be obtained with a $\Delta T \approx 55$ K between both self-images. Once the heater length has been chosen, the optimum width has been designed through 3D simulations based on the beam propagation method (BPM). Figure 1(b) shows the obtained results. It can be seen that a heater width of 3.7 µm is required to maximize the crosstalk above 20 dB. The transmission response as a function of the index variation is shown in Fig. 1(a).

Thermal simulations have also been performed using a 3D finite element method (FEM) to analyze the thermal crosstalk of the MMI structure and how it does affect to the resultant phase shift. The heater was located on top of a 700 nm thick silica upper cladding, just over the self-image on the MMI (see Fig. 2(a)). High thermal crosstalk can be observed due to the high silicon thermal conductivity of 149 W/(mK) [21]. In Fig. 2, a power consumption of 60.4 mW has been used to reach a $\Delta T \approx 55$K between the sides of the MMI structure and so the desired phase shift of one self-image over the other one. Figure 2(b) shows the temperature difference between both sides of the MMI structure along the propagation direction. Vertical left and right lines (red and yellow) shows the beginning and the end of the heater. Figure 2(c) depicts the phase shift taking into account the temperature difference reported in Fig. 2(b). It can be seen that the reached phase shift is above π radians. However, 60.4 mW is still a high value for low power applications and thus a solution to minimize the power consumption has been investigated.

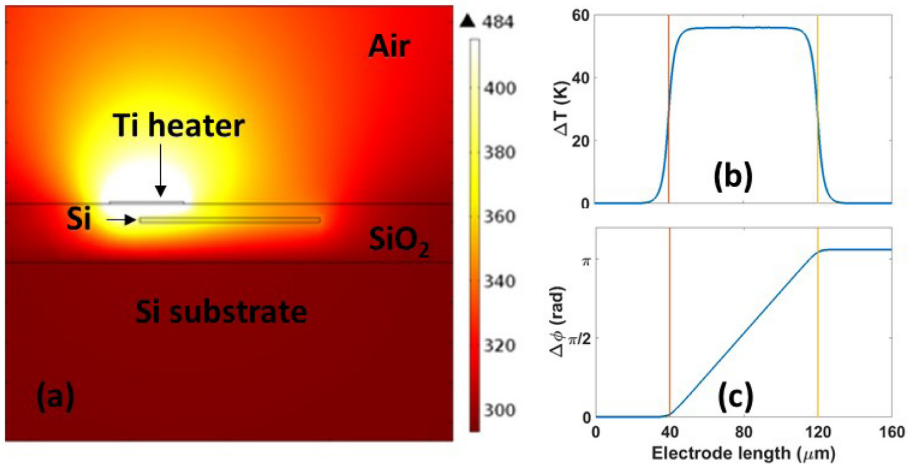

Fig. 2. (a) Heat distribution in a transversal cut of the MMI structure, (b) temperature difference between both sides of the MMI along the propagation direction and (c) accumulated phase shift obtained from the temperature difference. Results have been obtained for an applied electrical power of 60.4 mW.

In order to decrease the power consumption, it is necessary to use a thermal isolation between the self-images, which allows to reduce the thermal crosstalk. A silica trench has therefore been etched in the middle of the silicon MMI structure. The optimum location to minimize the impact on the MMI performance in terms of insertion loss is found to lie where the optical field is weak enough, that is, around 350 µm with respect to the z-axis as can be seen in Fig. 3(a). Once the position has been chosen, the optimum length and width of the silica trench has been designed. A tradeoff between minimizing the insertion losses and achieving a large thermal isolation has been found. The optimum size of the trench has been obtained for a trench length and width of 50 µm and 2 µm, respectively, causing an insertion loss of around 2 dB (see Fig. 3(b)). Further optimization of the MMI parameters was carried out so that the insertion losses were reduced from 2 to 0.5 dB by increasing the MMI length up to 616 µm. Figure 3(c) shows the optical field distribution of the optimized MMI structure with the silica trench. Despite the fact that the interference pattern is slightly distorted due to the trench presence, it remains without significant alterations.

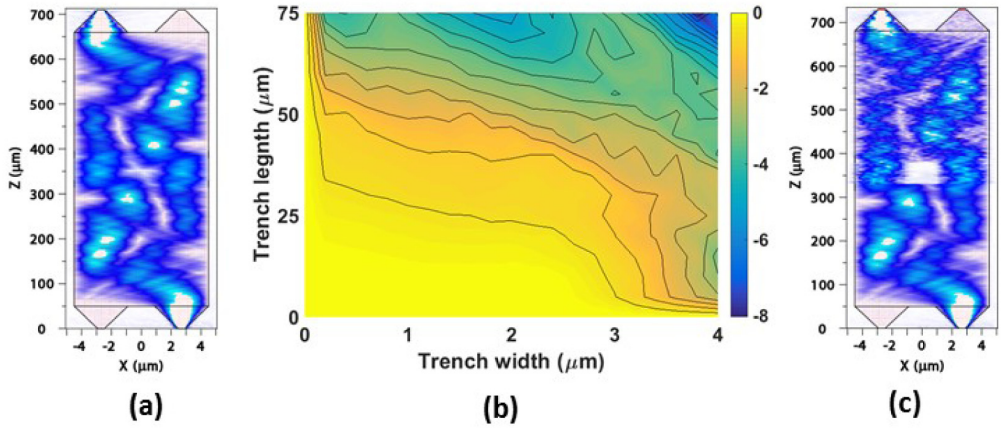

Fig. 3. (a) Optical field distribution in the conventional MMI structure. (b) Insertion losses versus silica trench dimensions. (c) Optical field distribution in the MMI structure with optimized silica trench.

Thermal simulations have also been carried out to analyze the effect of the trench on the thermal isolation and to eventually evaluate its impact on the power consumption. Figure 4(a) shows the heat distribution in the optimized MMI structure for the same transversal cut than in Fig. 2(a). It can be clearly seen that the heat is concentrated on the heater side owing the isolation gap unlike in the conventional MMI structure in which the heat spreads out along the silicon layer. The π radians phase shift was reached (Fig. 4(c)) in the optimized MMI structure with a power consumption of 35.4 mW, which means a reduction of approximately 45% compared with the conventional MMI structure without trench.

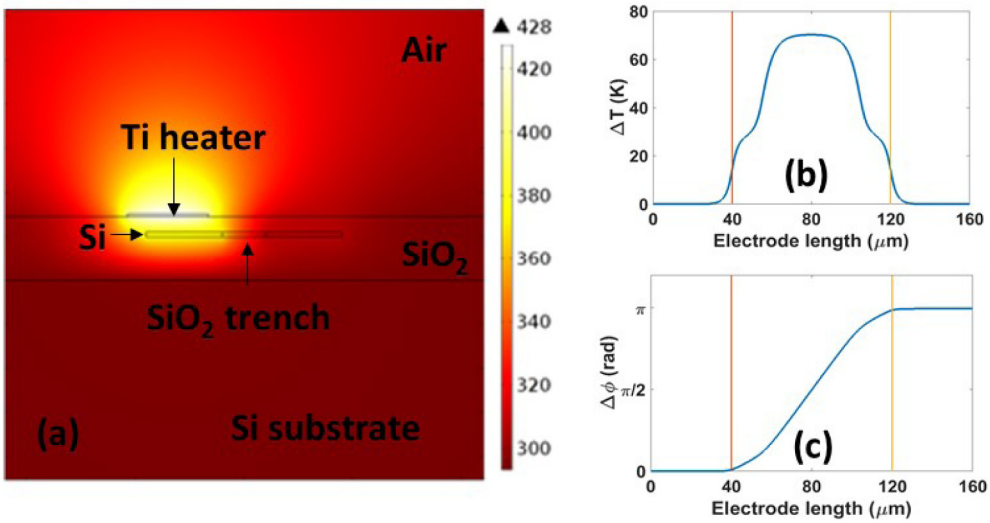

Fig. 4. (a) Heat distribution in a transversal cut of the MMI structure with silica trench, (b) longitudinal temperature difference between both sides of the MMI and (c) accumulated phase shift obtained from the temperature difference. Results have been obtained for an applied electrical power of 35.4 mW.

3. Design of the electrodes

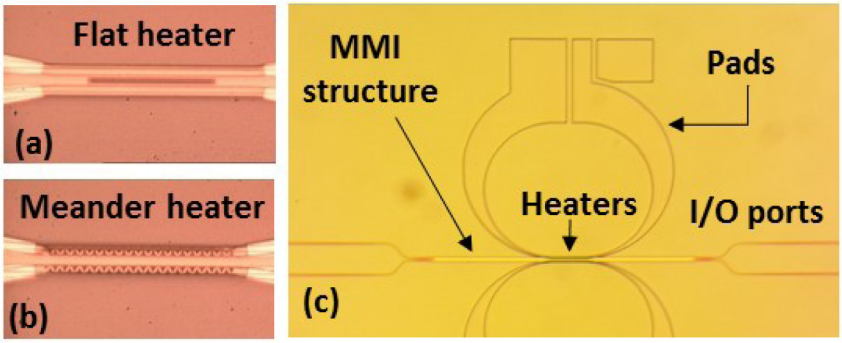

Fig. 5. (a) Flat heater in the MMI with the silica trench, (b) meander heater in the MMI without silica trench and (c) 2x2 switch with electrodes consisting of the copper pads and the titanium heaters on top of the MMI structure.

The switching performance can be further enhanced by optimizing the electrodes with the aim of improving the power consumption. Therefore, we have optimized both the heater and the electrodes. The difference between the electrode and the heater should be pointed out: the heater is the metal section designed to achieve a highly localized temperature in the MMI structure (see Figs. 5(a) and 5(b)), and the electrode includes the whole electrical circuit

consisting of the pads and the heater (Fig. 5(c)). Therefore, the electrodes can be defined as a combination of three resistances. Two resistances for each one of the pads, and the last one for the heater. To improve the performance of the electrode, the heater should dissipate the maximum amount of the total dissipated power.

The first design is focused on the flat heater (Fig. 5(a)) with an electrode fabricated only with titanium. From that simple design, two improvements are proposed: (i) using a meander shape for the heater (Fig. 5(b)), which will lead to an increase of the heater resistance, and (ii) replacing the titanium electrode pads by copper, which will reduce the resistance of the pads and thus the dissipated power that does not contribute to the phase change. Figure 5(c) shows the 2x2 switch composed by the copper pads and the titanium heaters on top of the MMI structure. Thermal simulations have also been carried out to determine the power consumption reduction achieved with the proposed electrodes. Table 1 summarizes the obtained simulation results. It can be seen that a power consumption reduction of around 25% has been achieved for the meander heater.

Table 1. Simulated power consumption for different heater and MMI configurations.

MMI structure	Flat heater	Meander heater
Without silica trench	60.4 mW	53.32 mW
With silica trench	35.54 mW	26.5 mW

4. Fabrication process

The optical switches based on the proposed MMI structures and electrodes were fabricated by using electron-beam lithography, inductive coupled plasma (ICP) etching and metal evaporation. The structures were fabricated on standard SOI samples from SOITEC wafers with a top silicon layer thickness of 220 nm and a buried oxide layer thickness of 2 µm. The fabrication is based on an electron beam direct writing process performed on a coated 100 nm hydrogen silsesquioxane resist film. The mentioned e-beam exposure was optimized in order to reach the required dimensions employing an acceleration voltage of 30 KeV and an aperture size of 30 µm.

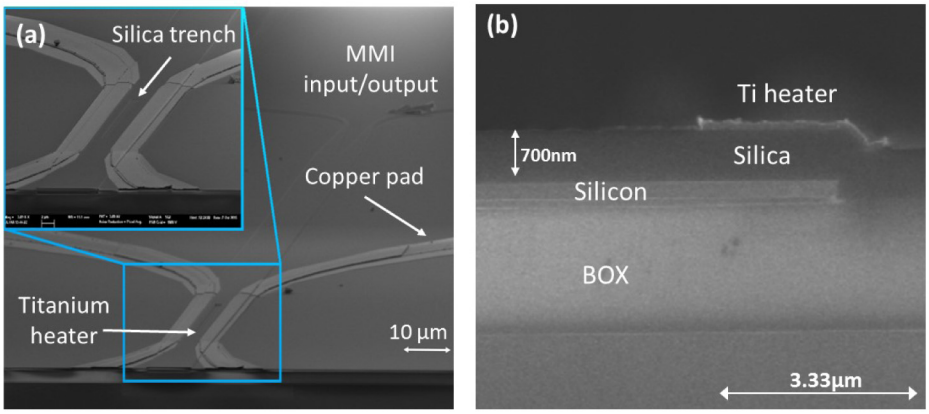

Fig. 6. (a) SEM image of the 2x2 MMI switch with the flat electrodes. The silica trench is shown in the inset. (b) Transversal SEM image of the MMI structure with the titanium heater.

After developing the hydrogen silsesquioxane resist using tetramethylammonium hydroxide as developer, the resist patterns were transferred into the SOI samples employing an also optimized ICP reactive ion etching process with fluoride gases. A 700 nm thickness silicon dioxide upper cladding was deposited on the SOI sample by using a plasma enhanced chemical vapour deposition (PECVD). Finally, the electrodes fabrication was implemented by two e-beam positive resist exposure (PMMA) prior to a metal evaporation and lift-off

processes. In the first exposure, 100 nm of titanium was deposited on the MMI areas while in the second exposure process the 100 nm copper pads were exposed. Figures 6(a) and 6(b) show scanning-electron microscope (SEM) images of the fabricated devices.

5. Experimental results

The fabricated devices have been characterized and their performance compared step by step. Figure 7(a) shows the optical power at both output ports as a function of the applied electrical power for the switches based on the MMI with and without the silica trench. In this case, titanium electrodes have been used in both MMI switches. As it can be observed, the required electrical power to switch between the bar and cross port is reduced by a factor of two approximately, from 254.2 mW to 122.7 mW.

Once this improvement has been demonstrated, the MMI structure with silica trench has been used to obtain the following results. Figure 7(b) shows the comparison between different electrodes based on copper and titanium pads. In this case, there is a significant power consumption reduction, from 122.7 to 36.5 mW due to the copper pads that demonstrates the huge amount of electrical power wasted when using titanium pads. The introduction of copper pads means a reduction close to 70%. Therefore, copper pads were considered for the final structures. Figure 7(c) shows the switching response for the different designed heaters: flat and meander. It can be seen that the power consumption is 36.5 mW for the flat heater and 24.9 mW for the meander heater. Therefore, a reduction of around 30% has been achieved in power consumption. Taking into account the initial power consumption of 245.2 mW and the final value of 24.9 mW, a 90% reduction has been demonstrated. Furthermore, there is an excellent agreement with the simulation results for both power consumption and optical performance as the impact in the insertion losses and crosstalk is very small.

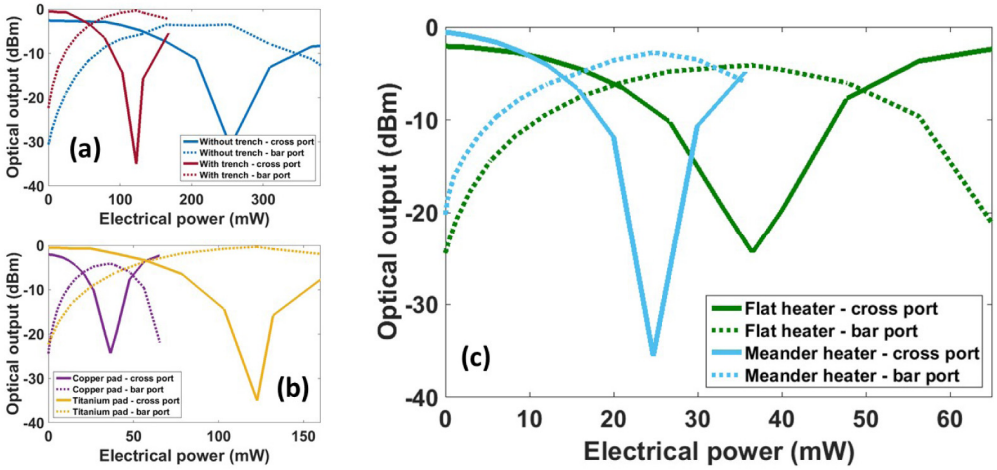

Fig. 7. Switching response of the MMI structure (a) with silica trench and without silica trench by using titanium pads, (b) with silica trench and electrodes with copper and titanium pads, (c) with silica trench and with the flat and meander heaters, both with copper pads.

In addition to power consumption, another important feature in optical switches is the time response. Therefore, the switching time of each structure has also been measured and results are shown in Table 2. In the cross port, the fall time is associated with the heating process while the rise time is associated with the cooling process. The opposite behavior occurs in the bar port. Clearly the cooling process is the limiting factor in the switching speed. Furthermore, it can be seen that the time response of the MMI structure with silica trench during the cooling process is around four time slower than in the MMI structure without trench. Such behavior is attributed to the small amount of heat that is transferred to the

environment due to the thermal isolation provided by the silica trench. On the other hand, it can also be observed that the heater geometry has a low dependence upon the switching time although slightly lower cooling times have been achieved for the meander heater. As a result, the meander heater is the best option as power consumption is also minimized, as depicted in Fig. 7(c).

However, there will be a trade-off between switching time and power consumption depending on the MMI structure. A very fast switching time of 1.19 μs with a power consumption of 54.4 mW ($P_\pi \cdot \tau \approx 65$ mW·μs) has been achieved by means of the MMI structure without silica trench and meander heaters. The power consumption can be reduced to 24.9 mW by introducing the silica trench in the MMI structure but at expenses of a higher switching time of 4.25 μs ($P_\pi \cdot \tau \approx 108$ mW·μs). Overall, the obtained results outperform the performance of MZI switches based also on the placement the heaters on top of the cladding layer [6, 9, 12].

Table 2. Switching time for measured structures.

MMI structure	**Without trench**		**With trench**	
Electrode structure	**Flat**	**Meander**	**Flat**	**Meander**
Heating time	0.53 μs	0.83 μs	0.45 μs	0.9 μs
Cooling time	1.7 μs	1.19 μs	4.3 μs	4.25 μs

The best obtained figure of merit is also comparable to thermo-optic MZI switches based on doping the silicon to directly build the heaters into the waveguide ($P_\pi \cdot \tau \approx 67$ mW·μs in [11]). By means of this approach, the efficiency of the thermal process is maximized and a figure of merit as low as 30.5 mW·μs has been recently demonstrated [10]. However, it should be pointed out that the fabrication complexity is notably increased as several implantation steps are required. In the proposed MMI switch, the fabrication is much simpler, the structure has a high robustness inherent to the MMI structure and the footprint is smaller than that of MZI-based switches.

6. Conclusion

The feasibility of developing silicon switches based on thermo-optically tunable MMI structures has been demonstrated. Thermal isolation between adjacent self-images, optimized heater shapes and the use of different metals for the heater and pads have been shown to be a key factor to minimize the power consumption. A trade-off between switching time and power consumption has also been shown. Overall, our results place 2x2 optical MMI-based switches among of the state-of-the art of silicon photonic switches based on the thermo-optic effect. Therefore, a new route has been opened to address the implementation of switching fabrics in silicon photonic technology.

Acknowledgments

Financial support from LEOMIS TEC2012-38540 and PROMETEOII/2014/034 projects is acknowledged. Álvaro Rosa also acknowledges the Spanish Ministry of Economy and Competitiveness for funding his grant. The authors also would like to thank the Electronic Microscopy Department at UPV for taking the SEM images.